CHAPTER 5: DEFORMABLE THORACIC CT IMAGES SEQUENCE REGISTRATION USING STRAIN ENERGY MINIMIZATION

The idea of deformable image registration (DIR) has been explored for a thoracic CT (computed tomography) image database of ten subjects. Thoracic CT image acquisition for clinical interventions requires a well-defined procedure which has already been underlined on the basis of field expertise and past experiences. Despite strict adherence to the procedure, the acquired images are prone to distortions and artefacts. This might happen due to organ motion during breathing process (at times even in breath-hold procedures), slight (even involuntary) movements or acquisition variations in supine and prone positions etc. An intensity differences based energy minimization method has been proposed. The moving image is transformed in the process such that it gets maximum alignment with the fixed image. This is achieved by energy minimization of the moving image in an iterative process. It is a simpler and more practical method for thoracic CT image registration than the prevalent approaches. This has been shown by lower mean registration errors for the patient data; the errors were as such axial: 0.283±0.08, coronal: 0.784±0.32 & sagittal: 0.66±0.2 pixels. This registration of moving image onto the fixed image in the sequence will help in minimizing the adverse effects of the otherwise present discrepancies, phase errors and discontinuity artifacts that might have crept in during the acquisition.

The proposed method begins with a pair of images of same dimensions; these images are part of an image sequence and have considerable temporal difference between them. The image sequence has been acquired as a part of the breathing

process. Of the two, image appearing earlier in the temporal timeline is considered as the target image and the one appearing later is considered as the source image. These both images represent the extremes of a breathing cycle such that the first image is full inhale and the last image is full exhale. These both images have their own specific energy signatures. Both these images have to be registered against each other. For the registration process, no direct comparisons between images are done; instead the source image is independently transformed in such a way that the transformed image has minimum intensity difference with the target image. It is an iterative process (as can be referred to in fig. 5.2), at each stage of which transformed versions of source image are compared to the target image for intensity difference of zero or less than a third decimal place value. If none of the two conditions are met, the transformed image goes into further transformation and the process continues until the source image is transformed to a level that it satisfies previously laid conditions. In our experiments, SNR (signal to noise ratio), PSNR (peak SNR), mean SSIM (Structural SIMilarity) index & NCC (Normalized Cross Correlation) have been used to estimate and establish increased similarity between the later transformed – target image pair in comparison to previous source – target image pair. Mean Registration Error (E_{T-R}) is used as the quantitative measure for the evaluation of performance. The E_{T-R} obtained for the dataset was found to be considerably lower than more traditional and prevalent transforms such as affine and b-splines based approaches.

5.1 Introduction

Organ motion pertaining to breathing can lead to image artefacts and position uncertainties during image guided clinical interventions. A particular case for

such image guided interventions (IGI) can be the radiotherapy planning of thoracic and abdominal tumours; the respiratory motion causes important uncertainties and is a significant source of error [Keall, P. J. *et al.*, 2006]. During a process of image acquisition, slight movement from the subject can translate into potential discrepancies in the acquired image sequence. Images in such an acquired sequence more than often end up out of sync and prove to be not of much use for both medical application and/or research purposes. A non-invasive method to describe lung deformations was proposed using NURBS surfaces based on imaging data from CT scans of actual patients [Tsui, B. M. W. *et al.*, 2000]. Image registration has recently started playing an important role in this scenario; it helps in the estimation of any motion caused due to breathing during acquisition and the description of the temporal change in position and shape of the structures of interest by establishing the correspondence between images acquired at different phases of the breathing cycle [Ehrhardt, J. *et al.*, 2011].

Image Registration is the alignment/overlaying of two or more images so that the best superimposition can be achieved. These images can be of the same subject at different points in time, from different viewpoints or by different sensors. This way the contents from all the images in question can be integrated to provide richer information. It helps in understanding and thus reducing the differences occurred due to variable imaging conditions. Most common applications of Image Registration include remote sensing (integrating information for GIS), combining data obtained from a variety of imaging modalities (combining a CT and an MRI view of the same patient) to get more information about the disease at once, cartography, image restoration etc. An image registration method targets to find the optimal transformation that aligns

the images in the best way possible. Image registration methods can be broadly classified into three basic classes, landmark (or point) based registration [Mcgregor, B., 1998; Rohr, K. *et al.*, 2001; Bookstein, F. L., & Green, W. D., 1993], segmentation based registration [Sull, S., & Ahuja, N., 1995; Feldmar, J., & Ayache, N., 1996; Jain, A. K. *et al.*, 1996] and the image intensity based registration [Szeliski, R., & Coughlan, J., 1994; Kybic, J., & Unser, M., 2003] depending on them being more cost efficient, fast and flexible over the others with respect to the image family it is being used to register and the application of the registration process. It is further categorized into two kinds based on the type of image it is being applied for. The two kinds of images are Rigid Images and Deformable Images. Rigid images are those of structures with rigid morphological properties e.g. bones, buildings, geographical structures etc. If the underlying transformation model allows local deformations, i.e. nonlinear fields' u(x), then it is called Deformable Image Registration (DIR) [Muenzing, S. E. A. *et al.*, 2014]. Deformable images are those of structures shape and size of which can be modelled after tangible physically deformable models [Sotiras, A. *et al.*, 2013]. Rigid image registration although is an important aspect of registration it is not the topic of discussion in this article. Since the discussion is about Medical Image Registration and almost all anatomical parts or organs of the human body are deformable structures, the concentration here is on DIR [Oliviera, F. P. M. & Tavares, J. M. R. S., 2012].

The proposed methodology is based on intensity based registration. It is fully automatic in its mode of operation and helps in faster and more accurate image registration in comparison to pure landmark based registration methods. This factor gives our method an upper hand when it comes to real-life medical

image registration problems. The intensity based energy minimization methodology seems more practical, stable and cost efficient for deformable images in comparison to landmark based or segmentation based methodologies for similar purposes. The method is simpler and faster than its contemporaries because the energy function is worked upon directly without solving large matrix system assemblies.

5.2 Background

The background study of this chapter initially includes a study of few most prominent proposed algorithms in the direction of study of the energy minimization based non-linear elastic image registration and its applications. Then the proposed methods relating to image registration of thoracic CT images are discussed. The propositions are categorically discussed keeping in mind their acute relevance and their year of occurrence. Propositions occurring at a later instant in timeline are given higher priority in terms of detailed discussion in comparison to earlier works to establish better context. These methods are compared in a tabular format in table D.1 in Appendix D.

Pennec and associates [Pennec, X. *et al.*, 2005] suggested a statistical regularization framework for non-linear registration based on the concept of Riemannian Elasticity. In the proposed method, elastic energy has been interpreted as the distance of the Green-St. Venant strain tensor to the identity, which in turn reflects the deviation of the local deformation from a rigid transformation. By changing the usually employed Euclidean metric for a more suitable Riemannian one, a consistent statistical framework has been defined to quantify the amount of deformation. These statistics were then used as parameters in a Mahalanobis distance to measure the statistical deviation from the observed

variability, giving a new regularization criterion that is called the statistical Riemannian elasticity. It was found that this new criterion is able to handle anisotropic deformations and is inverse-consistent. Preliminary results and observations showed that it can be quite easily implemented in a non-rigid registration algorithm.

Bao Zhang and associates [Zhang, B. *et al.*, 2011] proposed a three-dimensional elastic image registration methodology based on strain energy minimization with its application to prostate magnetic resonance imaging. The registration algorithm was also applied on ten sets of human prostate data, each with two typical deformation states (one with 0 cc of air and the other with 40–60 cc of air inflated in the endorectal coil balloon). There were a total of 200-400 landmarks used to derive the transformation depending on the size of each prostate. They described it as a novel 3-D elastic registration procedure that is based on the minimization of a physically motivated strain energy function that requires the identification of similar features (points, curves, or surfaces) in the source and target images. The Gauss-Seidel method was used in the numerical implementation of the registration algorithm. The registration procedure was validated on synthetic digital images, MR images from prostate phantom, and MR images obtained on patients. Registration errors were assessed by averaging the displacement of a fiducial landmark in the target to its corresponding point in the registered image. The registration error on patient data was 1.8±0.7 pixels. Registration also improved image similarity (normalized cross-correlation) from 0.72±0.10 to 0.96±0.03 on patient data. Registration results on prostate data in vivo demonstrated that the registration procedure could be used to significantly improve both the accuracy of localized therapies such as brachytherapy or

external beam therapy and can be valuable in the longitudinal follow-up of patients after therapy.

Ronald W. K. So and associates [So, R. W. K. *et al.*, 2011] proposed a technique for non-rigid image registration of brain magnetic resonance images using graph-cuts. A graph-cut based method was proposed for non-rigid medical image registration on brain magnetic resonance images. In this proposal the non-rigid medical image registration problem has been reformulated as a discrete labelling problem. They modelled the non-rigid registration as a multi-labeling problem by Markov random field. The image registration problem was therefore modeled by two energy terms based on intensity similarity and smoothness of the displacement field. The MRF energy was minimized using graph-cuts algorithm via α-expansions. The registration results of the proposed method were compared with two state-of-the-art medical image registration approaches: free-form deformation based method and demons method. In addition, the registration results were also compared with that of the linear programming based image registration method. The proposed method was found to be more robust against different challenging non-rigid registration cases with consistently higher registration accuracy than those three methods, and gives realistic recovered deformation fields.

Andrew R. Dykstra and associates [Dykstra, A. R. *et al.*, 2012] proposed a method which co-registers high-resolution preoperative MRI with postoperative computerized tomography (CT) for the purpose of individualized functional mapping of both normal and pathological (e.g., interictal discharges and seizures) brain activity. The proposed method accurately (within 3 mm, on average) localizes electrodes with respect to an individual's neuroanatomy. Furthermore,

they outlined a principled procedure for either volumetric or surface-based group analyses. The method was demonstrated in five patients' data with medically-intractable epilepsy undergoing invasive monitoring of the seizure focus prior to its surgical removal. Accuracy of the method was found within 3mm of average. The straight-forward application of this procedure to all types of intracranial electrodes, robustness to deformations in both skull and brain, and the ability to compare electrode locations across groups of patients makes this procedure an important tool for basic scientists as well as clinicians.

H. P. Heinrich and associates [Heinrich, H. P. *et al.*, 2013] proposed a MRF-Based Deformable Registration and Ventilation Estimation of Lung CT. In the proposed method three major challenges associated with lung ct registration viz. large motion of small features, sliding motions between organs and changing image contrast due to compression are addressed and potentially higher quality of discrete approaches is preserved. First, an image-derived minimum spanning tree is used as a simplified graph structure, which coped well with the complex sliding motion and allowed to find the global optimum very efficiently. Second, a stochastic sampling approach for the similarity cost between images is introduced within a symmetric, diffeomorphic B-spline transformation model with diffusion regularization. The complexity is reduced by orders of magnitude and enables the minimization of much larger label spaces. In addition to the geometric transform labels, hyper-labels are introduced, which represent local intensity variations in this task, and allow for the direct estimation of lung ventilation. The improvements are validated in accuracy and performance on exhale-inhale CT volume pairs using a large number of expert landmarks. The three challenges posed in the beginning are met.

Keita Nakagomi and associates [Nakagomi, K. *et al.*, 2013] proposed a segmentation based registration methodology which uses multi-shape graph cuts with neighbour prior constraints for lung segmentation from a chest CT volume. A novel graph cut algorithm has been proposed that can take into account multi-shape constraints with neighbor prior constraints, and reports on a lung segmentation process from a three-dimensional computed tomography (CT) image based on this algorithm. It is a novel segmentation algorithm that improves lung segmentation for cases in which the lung has a unique shape and pathologies such as pleural effusion by incorporating multiple shapes and prior information on neighbour structures in a graph cut framework. The efficacy of the proposed algorithm is demonstrated by comparing it to conventional one using a synthetic image and clinical thoracic CT volumes.

5.3 Method

5.3.1 Preparation

The dataset used comprised of a total (3×10)×10 i.e. 300 thoracic CT images across 10 subjects. All images were anonymized and all procedures followed were in accordance with the ethical standards of the responsible committee on human experimentation (institutional and national) and with the Declaration of Helsinki 1975, as revised in 2008 (5). Informed consent was obtained from all patients for being included in the study. All patients or legal representatives signed informed consent. The images lie between CT phases 0-5 i.e. end-inspiration to end-expiration in timestamp range t00→t05. The image dimensions lie between 396×396 to 432×400 pixels. There were 6 frames from a temporal thoracic image sequence each for every Anatomical Plane (AP) i.e. Axial (supine), Coronal and Sagittal for all the 10 subjects acquired simultaneously with a gap of 0.1 second

starting from time t= 0.1 to 0.6 seconds. All images were identified as $I_N^{AP}(x, y, t)$ where $\{N, t \in \mathbb{R}^+ | 1 \leq N \leq 10, 0.1 \leq t \leq 0.6\}$, (x, y) are the x & y coordinates in the Cartesian plane and AP signifies the three anatomical planes of view i.e. Axial (a), Coronal (c) and Sagittal (s). Suppose the 3rd frame from coronal AP for subject 'case 9', would be notified as $I_9^c(x, y, 0.3)$. A view of the image database is shown in the table 5.1 for representational purposes.

Table 5.1: All three anatomical viewpoints for all the 10 subjects at time t=0.1 & 0.6 sec

	ANATOMICAL PLANES (T & S Images)		
	Axial	**Coronal**	**Sagittal**
1	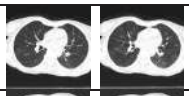	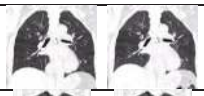	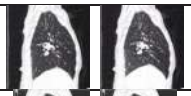
2	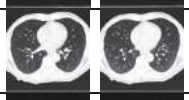		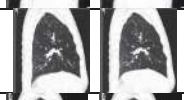
3	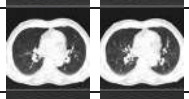		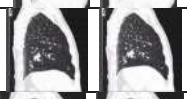
4	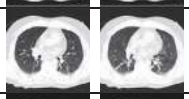	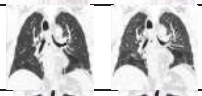	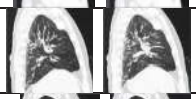
5	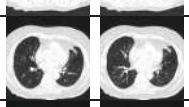	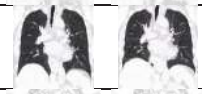	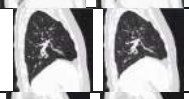
6	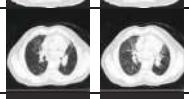	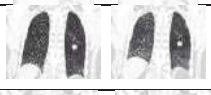	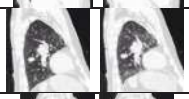
7	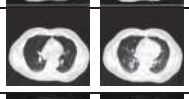	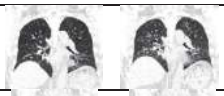	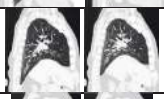
8	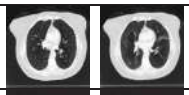		
9	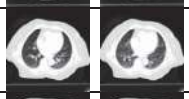		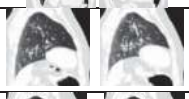
10	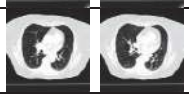	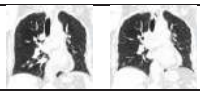	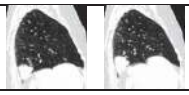

5.3.2 Proposed Methodology

What we have is a temporal sequence of images starting from time t=0.1 to t=0.6 seconds. It starts from the end- inspiration phase and continues up to the end-

expiration phase of the breathing cycle. The last image of the aforementioned sequence being diametrically most deformed with respect to the first image. We have proposed a method to register these two images with respect to each other. The two images are the target (T) and the source images (S) at t=0.1 and t=0.6 sec. respectively. These images belong to the same domain Ω and are related through a transformation T_R. This transformation is such that the resulting transformed image (S′) has the minimum energy distribution difference in terms of a similarity measure with the target image T, this has been shown in fig. 5.1. In simpler terms it can be stated as: 'a transformation sought such that the transformed image has minimum intensity difference with the target image'.

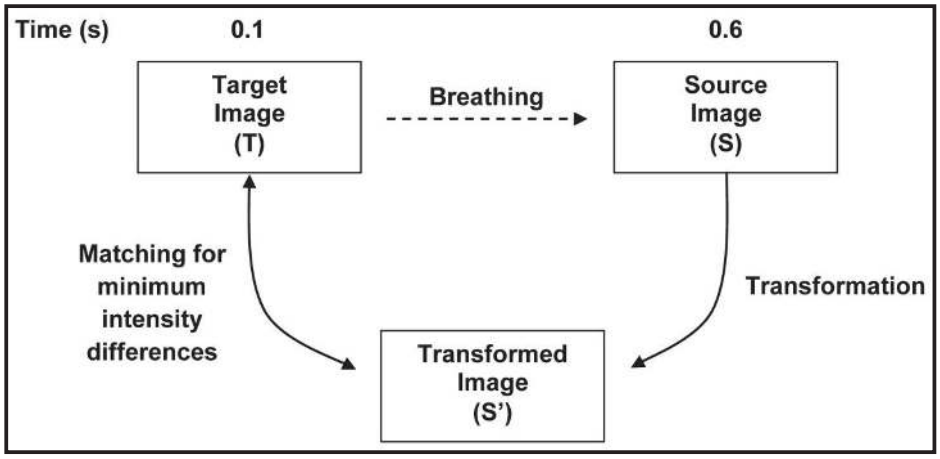

Figure 5.1: Overview of the proposed methodology

There is a potential energy associated with an elastic system at a time. Since, the images involved in the study are of a human body organ, they can be categorized as non-rigid or deformable images and the energy principles of elastic systems are applicable to this set of images. Potential energy of an elastic two dimensional system at static equilibrium is pure strain energy; it can be defined as [Ugural, A. C., & Fenster, S. K., 2003]:

$$U = \iint_{\Omega} {}^{1}/_{2} \left[\lambda e^2 + 2\mu\left(\varepsilon_x^2 + \varepsilon_y^2\right) + \mu\gamma_{xy}^2\right] d\Omega \tag{5.1}$$

where Ω is the image dimension, λ is the tensile stress (engineering constant), μ is the shear modulus, together they are called the Lame' constants; ε_x and ε_y are normal strains in the x and y directions respectively, γ_{xy} is the shear strain in the x-y plane pointing towards the y direction and 'e' is the unit change in image dimensions.

The Poisson's ratio value for Lung tissue averages close to 0.46 [Al-Mayah, A. et al., 2008; Brock, K. K. et al., 2005; Sundaram, T. A., & Gee, J. C., 2005, Zhang, T. et al., 2004]. In equation 5.1, the first term 'λe^2' can be ignored since it is two order lower than the rest of the terms. This makes the energy expression independent of tensile stress λ:

$$U = \iint_{\Omega} {}^{1}/_{2} \left[2\mu\left(\varepsilon_x^2 + \varepsilon_y^2\right) + \mu\gamma_{xy}^2\right] d\Omega$$

this can be further simplified to:

$$U = \mu \iint_{\Omega} \left[\left(\varepsilon_x^2 + \varepsilon_y^2\right) + {}^{1}/_{2}\,\gamma_{xy}^2\right] d\Omega \tag{5.2}$$

Suppose u, v are the displacements in x and y directions respectively. Normal strain ε_a is defined as $\frac{extension}{original\ \ lengt\,h}$ in the direction 'a' (a= x, y); shear strain γ_{ab} in the plane a-b would be the sum of angle of shear (for smaller degrees of shear). Thus, $\varepsilon_x = \frac{\partial u}{\partial x}$ and $\varepsilon_y = \frac{\partial v}{\partial y}$, similarly $\gamma_{xy} = \frac{\partial u}{\partial y} + \frac{\partial v}{\partial x}$. Exacting these values to equation 5.2:

$$U = \mu \iint \left[\left({}^{\partial u}/_{\partial x}\right)^2 + \left({}^{\partial v}/_{\partial y}\right)^2\right] dxdy + {}^{1}/_{2}\,\mu \iint \left[\left({}^{\partial u}/_{\partial y} + {}^{\partial v}/_{\partial x}\right)^2\right] dxdy \tag{5.3}$$

So, the expression for energy function 'U' in equation 5.1 has been reduced to strictly a strain energy function in equation 5.3, the equation 5.3 hence can be rewritten for U_{strain} as:

$$U_{strain} = \mu \iint \left[\left({}^{\partial u}/_{\partial x} \right)^2 + \left({}^{\partial v}/_{\partial y} \right)^2 \right] dxdy + {}^{1}/_{2}\,\mu \iint \left[\left({}^{\partial u}/_{\partial y} + {}^{\partial v}/_{\partial x} \right)^2 \right] dxdy \qquad (5.4)$$

The strain energy 'U_{strain}' minimization requires that over the image boundary conditions between the source and the target images:

$$\delta U_{strain} = 0 \qquad (5.5)$$

Such that the minimization constraint can be expressed in terms of intensity difference between the transformed image (S') and the target image (T) over the image dimensions' (Ω) as:

$$\int_{\Omega} (I_{S'} - I_T)\ \mathrm{d}\Omega = 0 \qquad (5.6)$$

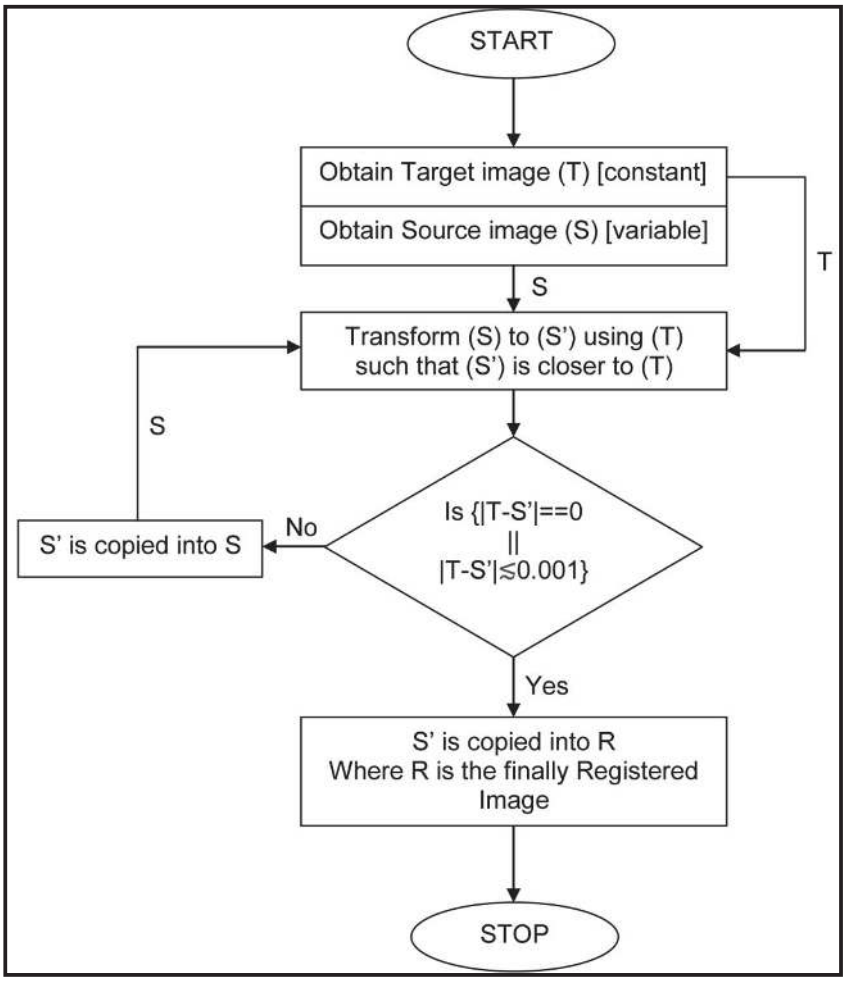

Figure 5.2: Flowchart of the iterative process in the registration procedure

It is an iterative process; as we can see in the fig 5.2, during the iteration, each time a transformed image is obtained, it is compared against the fixed image and an intensity difference mapping and value is calculated. These intensity differences are checked at each step. If very little or negligible change (say up to third decimal place) is observed, the iteration is stopped and the finally transformed image is considered as the required registered image. In case of progressively changing intensity differences for consecutive iterations, the iteration is continued until the stopping factor comes into play.

5.4 Results and Discussion

Iterative energy minimization using intensity differences across the image boundaries yield a transformed image (S') which was pitted against the actual target image (T) at different stages of the iteration to assess the level of transformation. Out of the ten subjects' data at hand, the coronal AP of subject 'case 3' has been chosen to elaborate and demonstrate the proposed technique with results. The transformed image (S') after the complete registration process showed an increase of 51.64% SNR (signal-to-noise ratio) value with respect to the target image (T) in comparison to the source image (S) with respect to target image. The change in PSNR (peak SNR) value was recorded at 41.64% in S'-T in comparison to S-T pair. A new metric called the SSIM (Structural Similarity) index has been used [Wang, Z. et al., 2004]. It has been used to estimate and measure the similarity between two images. It has been used as a deciding metric which would give a percentage similarity between the two images in question i.e. the fixed and the moving image and the fixed-transformed image pair. The mean SSIM index for the S-T pair was calculated at 0.4975, the same index for the S'-T pair came at 0.735. Along with similarity measures such as SNR, PSNR and m-SSIM, NCC (normalized cross-correlation) has been used to demonstrate as to how close the transformed image (S') has come to the target image (T) as a result of the registration process. The NCC value for S-T pair was estimated at 0.8817, for the S'-T pair it was calculated at a higher value of 0.9749 which further helps in establishing the closeness of the transformed image to the target source and hence, the proposed methodology as an efficient deformable image registration approach.

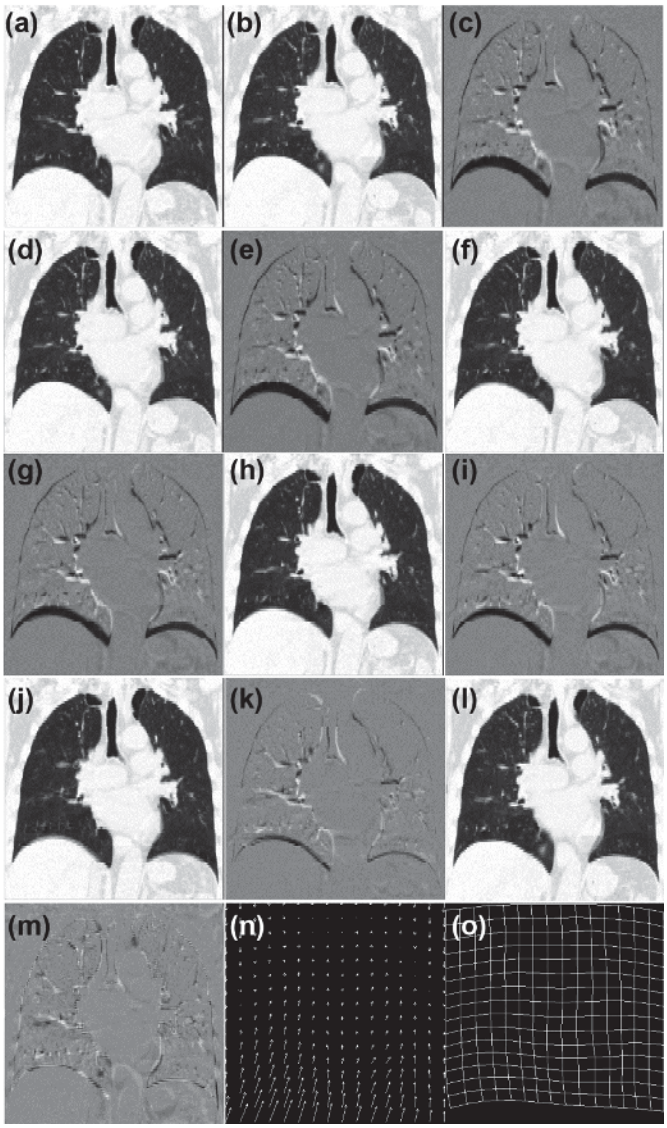

Figure 5.3: The iterative process graphical results on 'case 3' coronal AP

The earlier discussed iterative process and how it results in the finally registered image has been shown in the fig. 5.3. Figure 5.3(a) & (b) are the fixed and moving images respectively, they are also the diametrically opposite images of a breathing cycle (i.e. full inhale and full exhale) in a respiration process. Figure 5.3(c) is the intensity difference mapping (IDM) of (a) & (b) before the iteration starts. Transformation is applied to the moving image and transformed image is obtained. An IDM and corresponding value is calculated for the newly transformed moving image and the fixed image. Changes in IDM and value for

current and previous stage is observed, if the change is zero or negligible in comparison to the intensity difference value at either of the two stages of the iteration, the iteration is stopped there and last transformed image is the registered image. Figure 5.3(d) is the transformed image at the 7th iteration, 5.3(e) is its IDM with respect to the fixed image. In this particular instance of subject 'case 3', it took 174 iterations to obtain the finally registered image which is the fig. 5.3(l); 5.3(m) is the final IDM indicating minimal difference of the registered image with respect to the fixed image indicating a seamless and smooth registration process. Figures 5.3(f) and (g) are the transformed and IDM (with the fixed image) images at 20th iteration; figs. 5.3(h) and (i) are the transformed and IDM (with the fixed image) at the 55th iteration; similarly 5.3(j) and (k) are the same at the 130th iteration. Figure 5.3(n) and (o) are the deformation vector and deformation field representations respectively for the finally registered image.

Figure 5.4 shows the energy minimization process for subject 'case 3' coronal AP, the iterative process continues until a finally registered image is obtained at 174^{th} iteration (that is where the minimization process stops). The initial descent was observed as fast with respect to iterations until 110^{th} iteration, after which the minimization process progresses with diminutive changes in intensity differences. It finally picks up at 124^{th} iteration until to finally finish the process at 174^{th}.

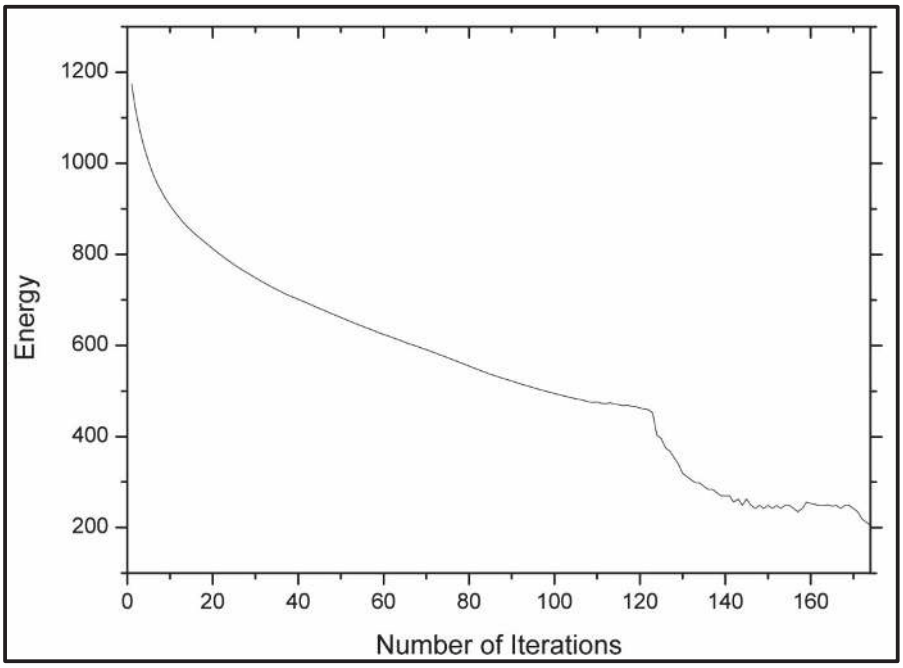

Figure 5.4: Energy minimization vs. Iterations for 'case 3' coronal AP

Table 5.2: SNR, pSNR, m-SSIM, NCC for all subjects under study from all APs; S-T is the source-target pair, R-T is registered-target pair for proposed method

Similarity estimation of S-T and R-T using various metrics for all subjects						
	Axial		Coronal		Sagittal	
	S-T	R-T	S-T	R-T	S-T	R-T
SNR (dB)	16.23±1.48	16.29±1.96	12.51±1.37	16.29±1.62	12.62±1.3	16.13±1.6
PSNR (dB)	20.52±1.14	20.58±1.62	15.35±1.36	19.13±1.6	16.33±1.5	19.83±1.8
m-SSIM index	0.744±0.05	0.742±0.04	0.49±0.08	0.58±0.12	0.57±0.13	0.64±0.14
NCC	0.964±0.01	0.969±0.01	0.85±0.03	0.93±0.02	0.89±0.03	0.95±0.03

The proposed technique was practically implemented on all the subject data at hand i.e. three anatomical positions across ten subjects. After obtaining the finally registered images for complete dataset, they were pitted against the fixed images

of their own sequence's respective sub-datasets. Similarity metrics such as SNR, pSNR, mean-SMIM index and NCC were calculated and compared for each S-T and R-T pairs for improvements (if any) which might suggest closeness of the registered image towards the fixed image. The observations are collected in table 2, they are average values over the complete dataset through all APs; all similarity metrics clearly seem to improve from S-T to R-T image pair for all subjects. Where there are significant changes in the case of coronal and sagittal APs, respective changes are not as notable in axial AP's data, this can be explained by usually comparatively smaller deformations in the 'anterior-posterior' direction.

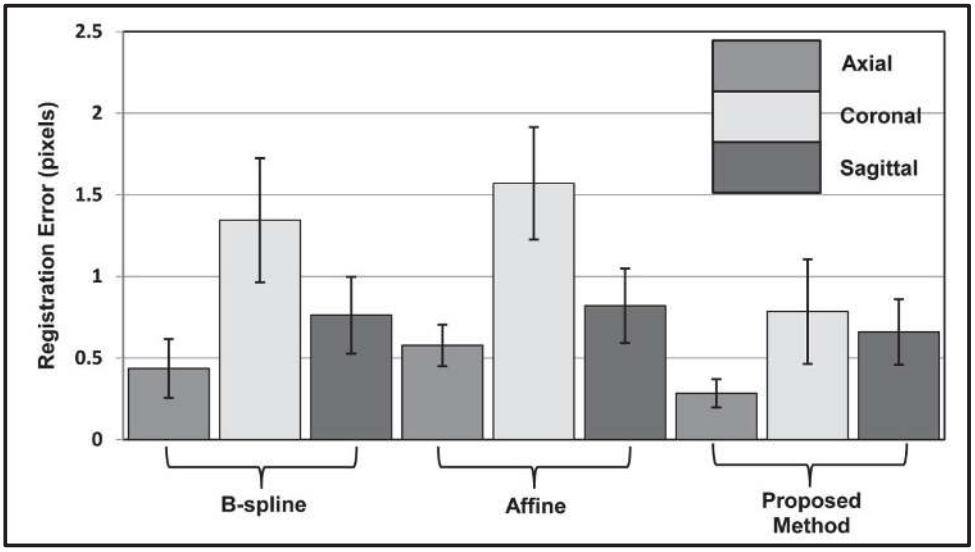

Figure 5.5: mean Registration error (pixels) for all 10 subjects through all APs

As can be seen in the figure 5.5, the mean registration errors (E_{T-R}) obtained for all the subjects involved in the test have been plotted through all three APs. Without the scope of any significant deformations comparable with coronal and sagittal APs, lowest mean registration errors were recorded for axial APs after

using all the tested transforms. The proposed method yielded least mean E_{T-R} (for all APs) while followed by b-spline and affine transforms in order. Not relying on landmark based features to establish correspondences instead applying purely intensity difference based energy minimization can be attributed for these results.

5.5 Conclusion

A novel, practically more feasible and accurate deformable image registration methodology for thoracic image sequences has been proposed. It could be a boon for real-life applications such as image acquisition for radiotherapy planning of thoracic lesions, dosimetric evaluation, tumour growth progression (with time) and determination of subject-specific deformable motion models.

An effort has been made to model elastic image deformations after real life 2D elastic object deformations such that all the constituents of that object are constantly in spontaneous motion and are not at equilibrium. Motion of 2D elastic objects due to internal forces has been used as an inspiration to determine deformations in thoracic CT images. Results from our study showed average target registration error of less than 1 pixel over the entire thoracic ct image volume. Such an accurate registration of thoracic ct images obtained in the deformed state can be useful in treatment planning and also for longitudinal evaluation of progression/regression in patients with lung cancer. Although the utility of this method has been shown for ct image volume, the method can be applied to images of any other imaging modalities as well.